Supporting Information for

Moiré metasurfaces with tunable near-infrared-I chiroptical responses for biomolecular chirality discrimination

Mengjia Cen [a,b,c], Jiawei Wang [a,b,c], Ming Cheng [a,b,c], Ziyan Lei [a,b,c], Ye Li [a,b,c], Zhenming Wang [a,b,c], Xueqian Zhao [a,b,c], Zixuan Wu [a,b,c], Huanian Zhang,*[,d,e] and Yan Jun Liu*[a,b,c]

[a]Department of Electrical and Electronic Engineering, Southern University of Science and Technology, Shenzhen 518055, China

[b]State Key Laboratory of Optical Fiber and Cable Manufacture Technology, Southern University of Science and Technology, Shenzhen 518055, China

[c]Shenzhen Engineering Research Center for High Resolution Light Field Display and Technology, Southern University of Science and Technology, Shenzhen 518055, China

[d]Zhejiang Lingkang Medical Equipment Co., Ltd, Wenling, 317500, China

[e]School of Physics and Optoelectronic Engineering, Shandong University of Technology, Zibo, 255049, China

*E-mail: huanian_zhang@163.com; yjliu@sustech.edu.cn

Contents:

Table S1: Comparison of the ratios (the resonance wavelength to the lattice period) from reported literatures.

Table S2: Comparison of relevant literatures for biomolecular chirality discrimination.

Fig. S6: CD spectra for ±45°-arranged moiré metasurfaces with and without proteins.

Fig. S7: Measured transmittance spectra without metagratings.

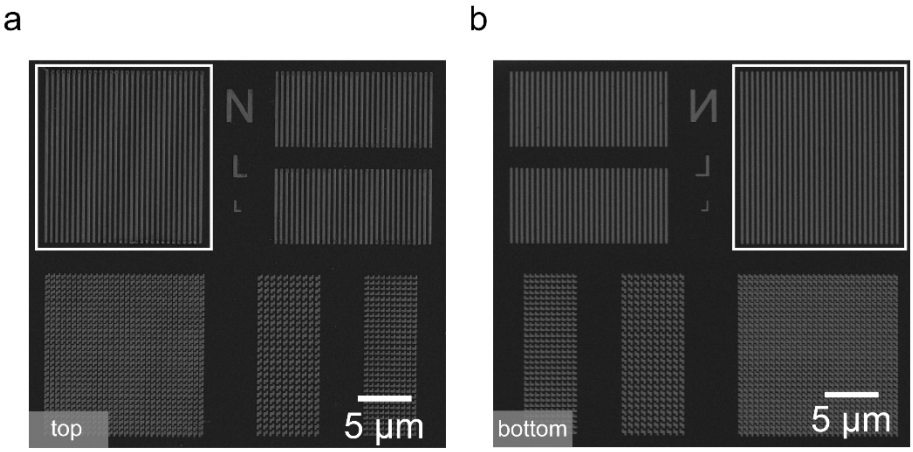

Fig. S1. (a) Top and (b) bottom SEM images of the fabricated suspended bilayer metasurfaces. It is worth nothing that we usually fabricate different types of nanostructures on the same substrate. The metagratings used in this work are highlighted by the white solid squares.

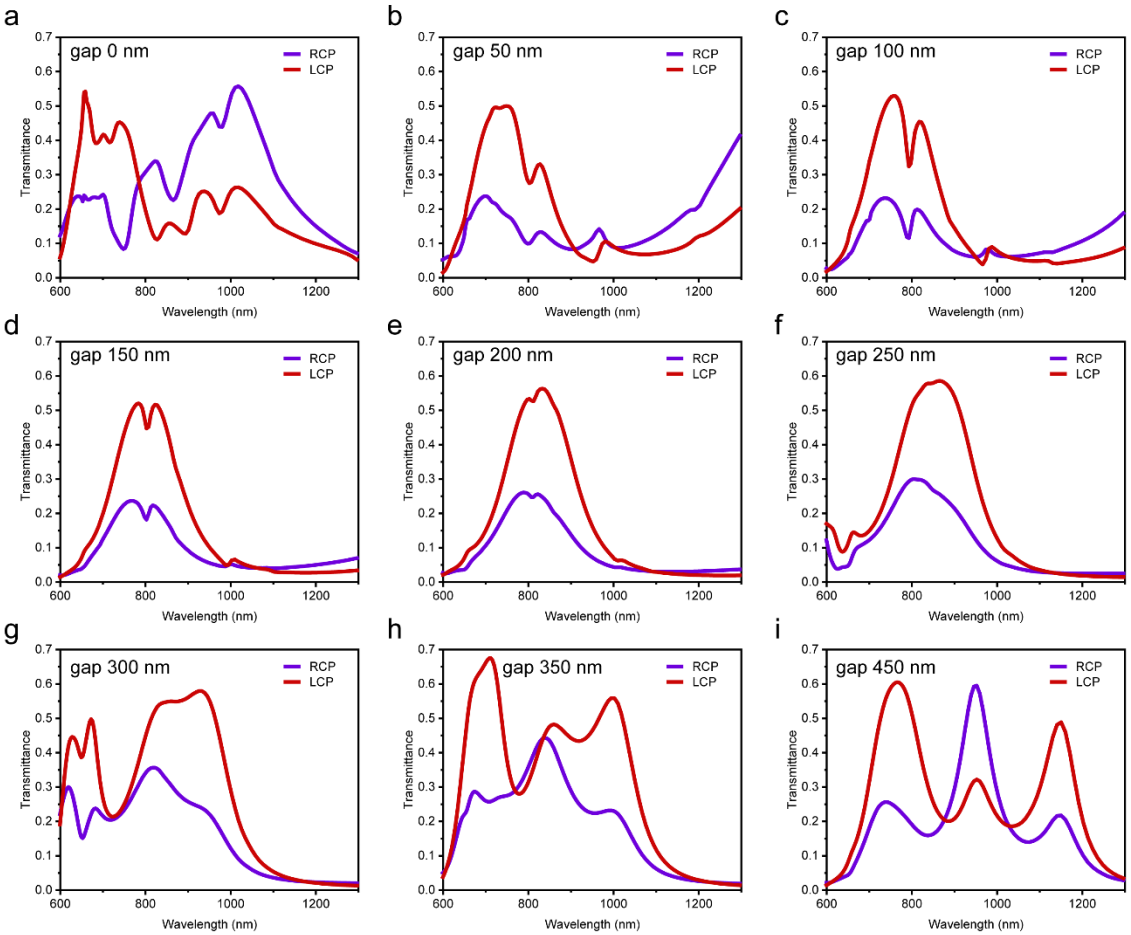

Fig. S2. (a–i) Simulated transmittance spectra of the +45°-arranged moiré metasurface for the gap distance from 0 to 450 nm.

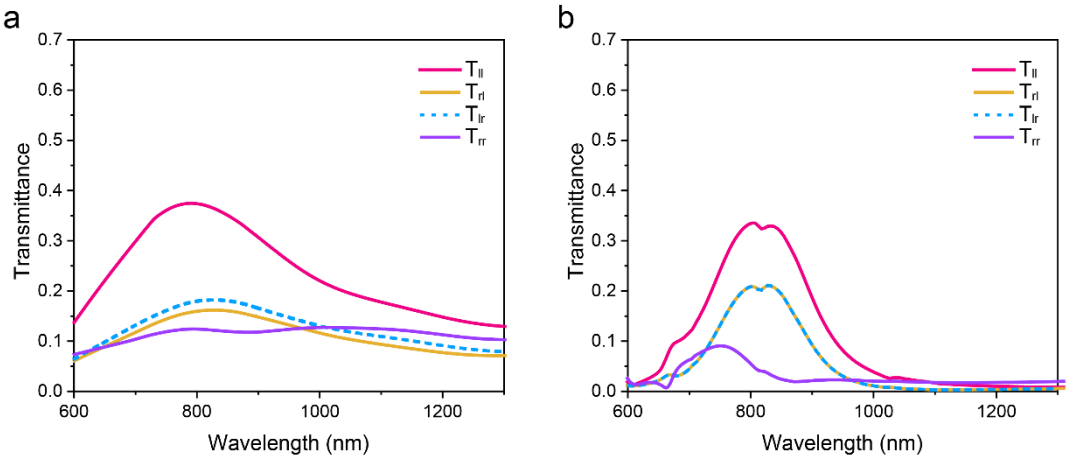

Fig. S3. (a) Experimentally measured and (b) correspondingly simulated transmittance spectra of various incident/output handedness combinations. T_{lr} (T_{rl}) refers to the intensity of the LCP (RCP) transmittance component under the incident RCP (LCP) light.

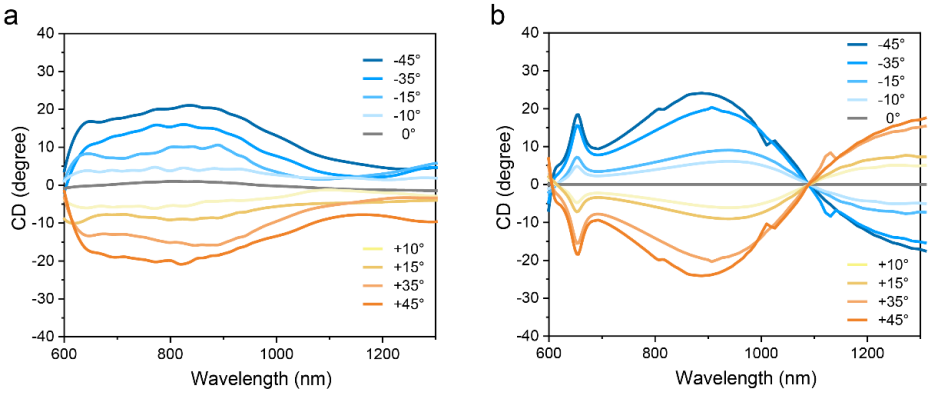

Fig. S4. (a) Measured and (b) simulated CD in degrees with twisted angle θ ranging from 45° to 0°.

The CD signal in degree is extracted by the following equation:[9,11]

$$CD = \tan^{-1}\frac{T_{\mathrm{RCP}} - T_{\mathrm{LCP}}}{T_{\mathrm{RCP}} + T_{\mathrm{LCP}}}, \tag{S1}$$

where T_{RCP} and T_{LCP} indicate the transmittance for incident RCP and LCP light. The measured CD spectra are in reasonable agreement with the simulated ones within the resonance range of interest. The differences between measured and simulated results above 1100 nm could be

mainly attributed to the low transmittance in this wavelength range. The small value of denominator in Eq. S1 makes pronounced large CD in the simulations, which actually can be ignored in the CD_T spectra. Thus, we focus more on the chiroptical responses around 825 nm.

Table S1. Comparison of the ratios (the resonance wavelength to the meta-atom period) retrieved from our work and other reported literatures.

Ref.	Moiré System (twisted nanostructures)	Circular Dichroism				Twisted angle	Period (nm)	Ratio
		Design Peak (nm)	RCP/LCP Transmittance	CD (deg)	CD_T			
[1]	particle chain arrays	1240	-	21	-	45°	365	3.39
[2]	nanorods	950	0.7/0.2	29.1	0.5	43.6°	250	3.8
[3]	nanoholes	700	-	-	0.1	15°	300	2.33
[4]	nanoholes	587	-	3.4	-	56.8°	535	1.10
[5]	Al meta-grating	508	0.65/0.3	20.2	0.35	45°	150	3.38
This work	suspended symmetry bilayer metagrating	825	0.498/0.224	20.9	0.274	45°	500	1.65
$CD(\text{deg}) = \tan^{-1}[(T_{RCP}-T_{LCP})/(T_{RCP}+T_{LCP})]$; $CD_T = T_{RCP}-T_{LCP}$								

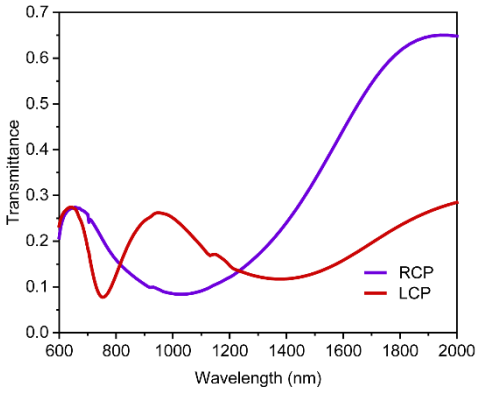

Fig. S5. Simulated transmittance spectra of the +45°-arranged moiré metasurface composed of two sheets of a single-layer metagrating.

Table S2. Comparison of biomolecular chirality discrimination from relevant literatures and our work.

Ref.	System	Analytes	Molecular dimension	ΔΔλ (nm)	sensitivity
[1]	Particle chain arrays (Moiré System)	Bovine Serum Albumin	21.8 nm×4.5 nm×14.3 nm	40	6 nm per fmol mm^{-2}
[6]	Dielectric cylinders	Phenylalanine	-	-	200 nm thick layer
[7]	Quantum dots with chiral metamaterials	Streptavidin	4.6nm×9.4 nm×10.5 nm	-	600 zmole
[8]	Nanoholes (Moiré System)	Glucose	-	1.9	180 femtogram
[9]	Twisted Au nanoraods	Concanavalin A	7.0 nm×11.7 nm×12.1 nm	-	55 zmole
[10]	Chiral metasurfaces	Shikimate kinase	6.4 nm×6.4 nm×9.2 nm	8	picogram level
[11]	Suspended bilayer chiral metasurfaces	Bovine Hemoglobin	7.9 nm×11.1 nm×6.5 nm	-	22.2 zmole
[12]	Nanoholes (Moiré System)	Concanavalin A	7.0 nm×11.7 nm×12.1 nm	2.5	picogram level
[13]	Chiral metasurfaces	Concanavalin A	7.0 nm×11.7 nm×12.1 nm	1.9	251 picogram
This work	Suspended symmetric bilayer meta-grating (Moiré System)	Bovine Hemoglobin	7.9 nm×11.1 nm×6.5 nm	34.7	1.07~1.83 nm per fmol mm^{-2}
		Bovine Serum Albumin	21.8 nm×4.5 nm×14.3 nm	54.2	2.1~10.17 nm per fmol mm^{-2}
		Concanavalin A	7.0 nm×11.7 nm×12.1 nm	12.1	0.60~1.03 nm per fmol mm^{-2}

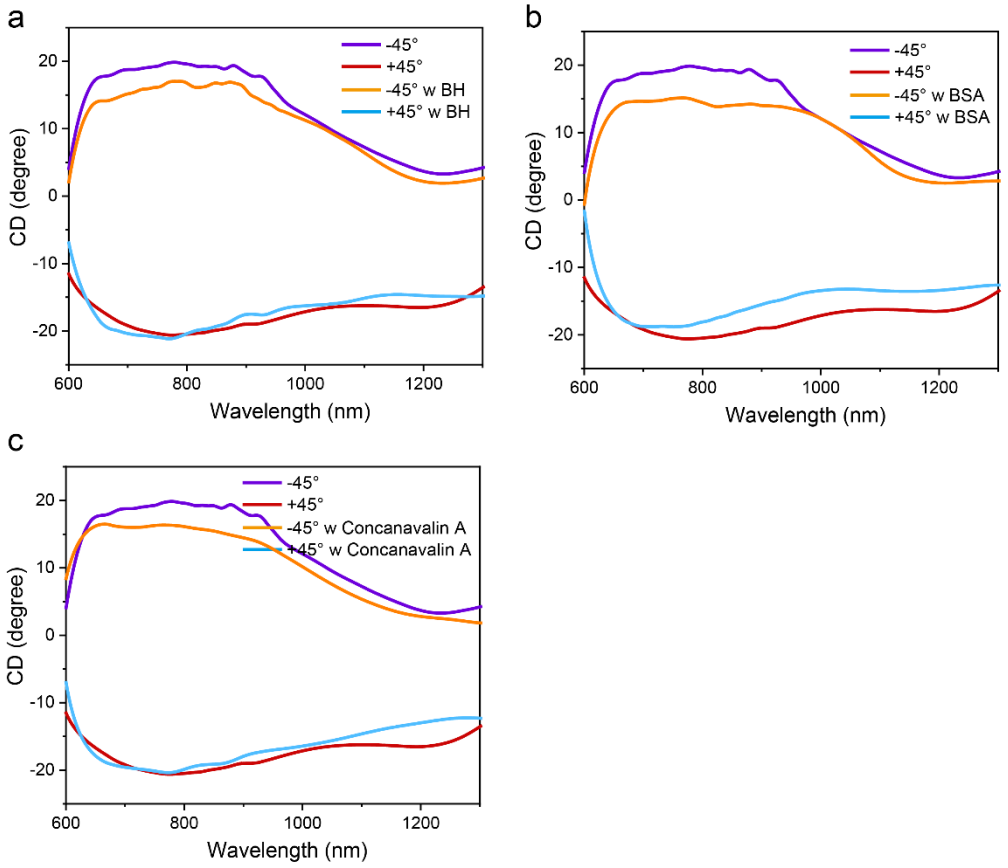

Fig. S6. (a–c) CD spectra for ±45°-arranged moiré metasurfaces with and without (a) BH, (b) BSA and (c) Concanavalin A, respectively.

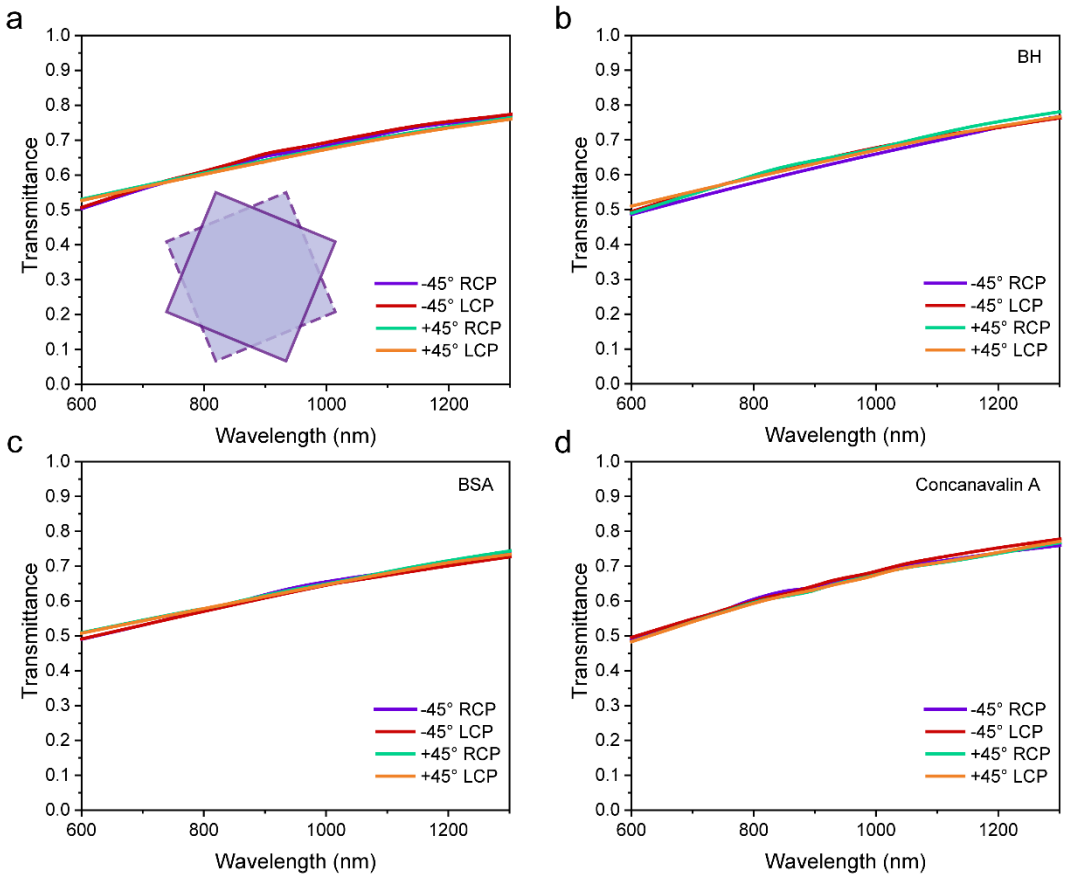

Fig. S7. Measured transmittance spectra of bilayer Si_3N_4 membranes (a) without and (b–d) with proteins including (b) BH, (c) BSA and (d) Concanavalin A, respectively.

References

1. P. T. Probst, M. Mayer, V. Gupta, A. M. Steiner, Z. Zhou, G. K. Auernhammer, T. A. F. König and A. Fery, *Nat. Mater.*, 2021, **20**, 1024–1028.
2. B. Lyu, Y. Li, Q. Jia, H. Li, G. Yang, F. Cao, S. Kou, D. Liu, T. Cao, G. Li and J. Shi, *Laser Photon. Rev.*, 2023, **17**, 2201004.
3. Z. Wu, X. Chen, M. Wang, J. Dong and Y. Zheng, *ACS Nano*, 2018, **12**, 5030–5041.
4. M. K. Chen, J. C. Zhang, C. W. Leung, L. Sun, Y. Fan, Y. Liang, J. Yao, X. Liu, J. Yuan, Y. Xu, D. P. Tsai and S. W. Pang, *Nanophotonics*, 2023, **12**, 2479–2490.

5. J.-G. Yun, S.-J. Kim, H. Yun, K. Lee, J. Sung, J. Kim, Y. Lee and B. Lee, *Opt. Express*, 2017, **25**, 14260.
6. J. García-Guirado, M. Svedendahl, J. Puigdollers and R. Quidant, *Nano Lett.*, 2020, **20**, 585–591.
7. M. Hajji, M. Cariello, C. Gilroy, M. Kartau, C. D. Syme, A. Karimullah, N. Gadegaard, A. Malfait, P. Woisel, G. Cooke, W. J. Peveler and M. Kadodwala, *ACS Nano*, 2021, **15**, 19905–19916.
8. Y. Liu, Z. Wu, P. S. Kollipara, R. Montellano, K. Sharma and Y. Zheng, *ACS Nano*, 2021, **15**, 6448–6456.
9. Y. Zhao, A. N. Askarpour, L. Sun, J. Shi, X. Li and A. Alù, *Nat. Commun.*, 2017, **8**, 14180.
10. R. Tullius, A. S. Karimullah, M. Rodier, B. Fitzpatrick, N. Gadegaard, L. D. Barron, V. M. Rotello, G. Cooke, A. Lapthorn and M. Kadodwala, *J. Am. Chem. Soc.*, 2015, **137**, 8380–8383.
11. M. Cen, J. Wang, J. Liu, H. He, K. Li, W. Cai, T. Cao and Y. J. Liu, *Adv. Mater.*, 2022, **34**, 2203956.
12. Z. Wu and Y. Zheng, *Adv. Opt. Mater.*, 2017, **5**, 1700034.
13. A. S. Karimullah, C. Jack, R. Tullius, V. M. Rotello, G. Cooke, N. Gadegaard, L. D. Barron and M. Kadodwala, *Adv. Mater.*, 2015, **27**, 5610–5616.